Realistic kinetic Monte Carlo study of the surface phase reconstruction

M. I. Monine and L. M. Pismen
Department of Chemical Engineering Technion, 32000 Technion City, Haifa, Israel;
Minerva Center for Nonlinear Physics of Complex Systems, Haifa, Israel;
and Institute of Catalysis Science and Technology, Technion, 32000 Haifa, Israel
(Received 21 July 2003; revised manuscript received 3 November 2003; published 27 February 2004)

Reversible $1\times1\rightleftharpoons1\times2$ reconstruction of Pt(110) surface is studied with the help of a kinetic Monte Carlo model. Activation energies of the allowed atomic steps are estimated using available computational and experimental data, and some discrepancies are reconciled to fit macroscopic data on surface reconstruction. Both energies of the various atomic configurations and activation energies depend on CO coverage and are estimated with the account of Pt-CO binding energies and repulsive interactions on adjacent sites. The model well reproduces both scanning tunneling microscopy results obtained for a clean 1×2 surface and available macroscopic data on $1\times1\rightleftharpoons1\times2$ reconstruction.

DOI: 10.1103/PhysRevE.69.021606 PACS number(s): 68.43.−h, 82.65.+r, 68.35.Ct

I. INTRODUCTION

It is well known that (110) and (100) surfaces of many transitional metals undergo reversible surface reconstruction which can be lifted by some adsorbates, e.g., CO or NO [1–4]. The reconstruction reduces the surface energy of a clean (110) surface of a face-centered cubic (fcc) lattice of such metals as Rh, Pd, Ir, Pt, Au, Ag, etc., by creating a ''missing row,'' or 1×2, structure with the sides of the rows forming (111) facets. Since the (111) structure has a lower surface free energy, the geometries exposing (111) facets (including also higher-order $1\times n$ superstructures) are favored thermodynamically [5–7]. Reconstruction into a close-packed 1×1 configuration takes place under the action of adsorbates, such as CO. The adsorbate-induced surface phase transition (SPT) controlled by the CO coverage provides the basic mechanism of rate oscillations and pattern formation in $CO+O_2/Pt$ reaction under low pressure [4,8].

Detailed studies of nanoscopic mechanisms of adsorbate-induced surface phase transitions, including substrate restructuring and microfaceting, taking place in the course of kinetic oscillations on Pt(110) became possible with the development of a variety of high resolution experimental techniques, such as low energy electron diffraction, reflection high energy electron diffraction, field ion microscopy, x-ray photoelectron diffraction, as well as scanning tunneling microscopy (STM) [1,2,9–17].

STM studies of Pt(110) surface demonstrated reversible reconstruction of an ordered missing row 1×2 structure into a 1×1 configuration via a ''hole eating'' mechanism under CO exposure [1,16]. Recent experiments have resolved dynamics of single Pt adatoms or clusters on the 1×2 surface of Pt(110) [12–15]. Statistical treatment of the recorded STM images allows us to estimate activation barriers and rates of elementary atomic jumps [18]. More data on surface structure and dynamics are provided by quantum chemical computations using density functional theory (DFT) and embedded atom method in order to predict binding energies of atoms on the surface or in the crystal bulk [19–23].

Dynamical simulations of the SPT implement various modifications of the Monte Carlo (MC) method [24–30]. The simulations are commonly based on an importance-sampling algorithm where transition probability of a single atomic step depends on the respective energy gain. Application of this method to surface reconstruction processes ensures rapid relaxation to an equilibrium state. Dynamics of Pt adatoms and surface restructuring can be modeled, however, more realistically with the help of kinetic Monte Carlo (KMC) technique where transition probabilities are calculated taking into account activation barriers, rather than just energies of the original and final atomic configurations [31].

This paper presents a realistic KMC study of the $1\times2\rightleftharpoons1\times1$ reconstruction of Pt(110) surface. We start in Sec. II with a brief review of recently published data on dynamics of adatoms and small clusters on Pt single crystal surfaces. Notwithstanding some contradictions in published data, we make an attempt to extract information necessary for KMC computations from the available data obtained for specific cases (surface diffusion of adatoms and clusters, dissociation of clusters) and use them to reproduce the reconstruction scenario in whole.

In our study we have developed a hybrid model combining a nanoscopic mechanism of the SPT and macroscale dynamics of CO coverage on the surface. The model to be described in Sec. III is based on a KMC algorithm using realistic activation barriers for adatom jumps. The barriers, as well as values of Pt-Pt and Pt-CO binding energies, have been extracted from the STM data and theoretical calculations. The model takes into account inhomogeneous distribution of CO on the surface. Our choice of the model parameters, as well as an application of the developed model to simulation of the $1\times2\rightleftharpoons1\times1$ transition under various thermodynamical conditions and comparison of the results with experimental measurements, is discussed in Sec. IV.

II. REVIEW OF EXPERIMENTAL AND THEORETICAL DATA

One can distinguish the following basic types of Pt adatom jumps [12,15,19,22,23,32]: (i) ''vertical'' or ''horizontal'' jumps (along or across the [110] rows, respectively) and ''diagonal'' jump; (ii) ''leapfrog'' (LF) mechanism

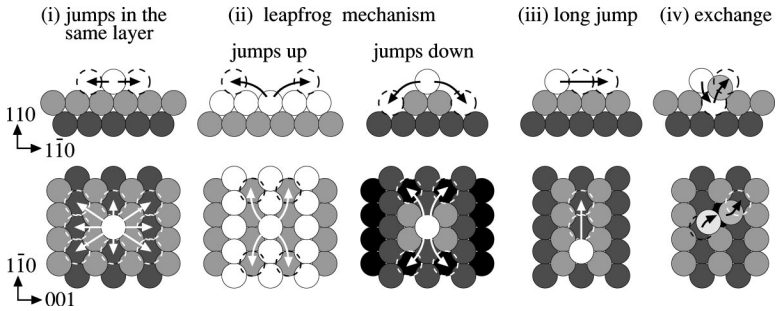

FIG. 1. Diffusion mechanisms of Pt adatoms: single jumps in the same layer (i), hopping up/down to the layer above/below (ii), long jump (iii), and exchange mechanism (iv). The first three panels show atomic jumps allowed in our model. The central atom can move to any available vacant position in the same layer (up to eight positions) through either vertical, horizontal, or diagonal jump (i). An atom can also hop to one of the closest available positions on the layer above or below (up to four positions on each layer) through the leapfrog mechanism (ii). The last two panels show the mechanisms (iii) and (iv), which are not considered in the model.

through hopping up or down to the layer above or below; (iii) ''long jumps'' along the [110] rows, i.e., adatom diffusion spanning several neighboring lattice sites; (iv) exchange mechanism through replacing a substrate atom. These diffusion paths are shown in Fig. 1. Selected values of activation barriers for single adatom jumps on a clean Pt(110) surface are summarized in Table I. The theoretical results and experimental data slightly differ. Nevertheless, the data clearly show that simple diffusion of Pt atoms [type (i)] on a close-packed 1×1 surface is more rapid than that on the 1×2 surface. A double jump [type (iii)] in channels of the 1×2 surface is characterized by a higher activation barrier than that for the single vertical jump. The exchange mechanism [type (iv)] has the highest barrier, since it involves activation of two Pt atoms. We assume that long jumps and exchange mechanisms [types (iii) and (iv)] can be presented as a combination of single atomic jumps [types (i) and (ii)]. Therefore, we shall consider only jumps in the same layer and LF hopping up/down as the main mechanisms of diffusion of Pt adatoms.

TABLE I. Activation barriers for diffusion of single adatoms on a Pt(110) surface.

Mechanism	Activation energy (eV)	Reference	Notes
''Vertical''	0.53	[23]	1×1 surface, theory
displacement	0.6	[18,19]	1×1 surface, theory
	0.81	[12]	1×2 channels, STM
	0.78	[1]	Reconstruction, STM
''Horizontal''	0.78	[1]	Reconstruction, STM
displacement	1.0	[1]	Defect formation, STM
LF, hopping up	0.76	[22]	Theory
	0.91	[14]	STM
	0.98	[23]	Theory
LF, hopping down	0.7	[14]	STM
	0.7	[23]	Theory
Double jumps in [1$\bar{1}$0] channels	0.89	[13]	1×2 surface, STM
Exchange across [1$\bar{1}$0] channels	1.09	[32]	Theory

Another kind of process involving adatom jumps is self-diffusion of one-dimensional (1D) clusters in [110] troughs (channels) of Pt(110)(1×2). Three basic mechanisms of cluster diffusion (involving usually 2–5 atoms) have been detected in recent studies [12,14,15,19,23,32]: concerted motion, when all atoms of the cluster move simultaneously over bridge sites; LF, when a back atom of the cluster jumps up, diffuses along the remainder or the cluster, jumps down, and connects to another end of the cluster; motion via exchange mechanism, when the penultimate atom of the cluster is pushed up by the last one and diffuses along the cluster like in the LF case. A comparison of the values presented in Table I with the available data on the cluster dynamics [23] shows that single adatoms are much more mobile than 1D clusters in 1×2 channels. The barrier for the concerted motion of clusters increases with increasing chain length from 1.55 eV for three atoms to 2.48 eV for five atoms in the cluster. The activation barrier of the exchange mechanism also increases with increasing size of the cluster from 1.30 eV for three atoms to 1.36 eV for five atoms. Diffusion of clusters via the LF mechanism is limited by the LF events of edge atoms, but this process is preferred to the concerted motion or exchange mechanisms. An adatom hopping up according to the LF mechanism moves along the cluster much faster than a monomer in a 1×2 channel. The difference between the activation barriers for the adatom migrating on a clean 1×1 surface (0.53 eV [23]) and in [110] channels (0.81 eV [12]) can be attributed to the influence of wall atoms.

In order to calculate the activation barriers, one needs to know, first of all, the energy of an initial atomic configuration. This energy can be evaluated by adding up Pt-Pt binding energies between the nearest neighboring (NN) atoms in vertical and horizontal directions (E_v and E_h, respectively). In the case of CO adsorption, Pt-CO binding energies ($E^{\text{Pt-CO}}$) and CO-CO repulsive interactions ($E^{\text{CO-CO}}$) should also be included. The respective data are presented in Table II. The data on Pt-Pt interactions [16,22,26] are in good mutual agreement. The linear dependence of $E^{\text{Pt-CO}}(n)$ on the coordination number of Pt atoms n fits the theoretical values of CO chemisorption energy [16]. The information obtained from time-dependent STM observations allows us to estimate interactions between NN atoms. It turned out that some

TABLE II. Pt-Pt, Pt-CO binding energies and CO-CO interaction.

Pt-Pt binding energies			
E_v (eV)	E_h (eV)	Reference	Method
−0.2	0.033	[26]	Theory
−0.225	0.05	[16]	Theory
−0.07		[15]	STM
−0.21		[22]	Theory
Pt-CO chemisorption energy			
	$E^{\text{Pt-CO}}(n)$ (eV)	Reference	Method
	$-3.84714+0.268929\,n$, $n=5,\ldots,10$	[16]	Theory
CO-CO repulsive interaction			
	$E^{\text{CO-CO}}$ (eV)	Reference	Method
	0.03	[16]	Theory

NN interaction energies which can be extracted from the STM statistics disagree with theoretical results. For instance, E_v for a dimer has been evaluated by Feibelman as −0.21 eV (DFT, Ref. [22]), which is three times larger than the value −0.07 eV following from the STM experiment by Linderoth *et al.* [15]. The authors suggest that this discrepancy may be attributed to CO impurities in the experiment.

The presented values of the activation barriers for single atomic jumps, as well as the binding energies, have been adjusted to our KMC model. It should be noted, however, that there is still a distinct lack of data on the influence of adjacent substrate atoms, as well as CO molecules adsorbed at NN sites, on the mobility of single Pt adatoms. This necessitates fitting certain parameters as explained in more detail in Sec. IV.

III. HYBRID MODEL

A. Representation of a Pt(110) surface

Our KMC computations involve single jumps of Pt atoms to vacant neighboring positions. Only five kinds of paths will be allowed: along and across the [110] direction (called, respectively, vertical and horizontal), diagonal and hopping up or down via the LF mechanism (see Fig. 1). We do not consider explicitly long jumps and diffusion of clusters via promotion and concerted motion, which, however, can be effected through combination of the allowed elementary steps. The diagonal jump can be introduced instead of a displacement via an exchange mechanism.

By our definition, the (110) surface of fcc lattice consists of $2N^2$ nodes; each of them is marked by an integer L defining the upper occupied level, as shown in Fig. 2. Only atoms occupying free top sites (i.e., not covered by any neighboring atom in the higher layer) are allowed to move. More details on computation of atomic jumps and the model algorithm are presented in the Appendix. The simulations have been carried out on lattices consisting of 2×50^2 and 2×100^2 atoms.

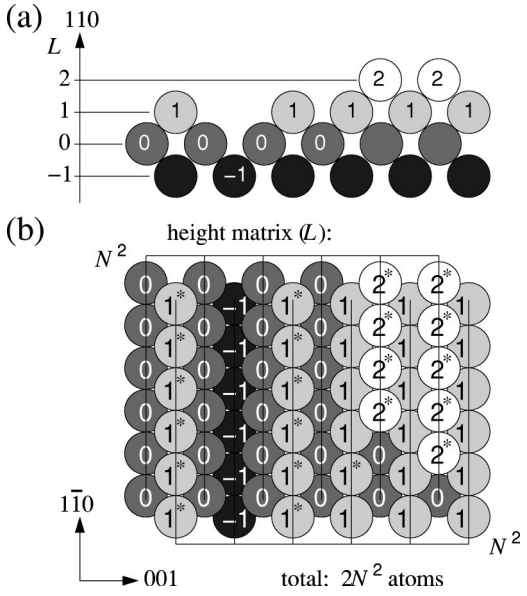

FIG. 2. Representation of the Pt(110) surface. (a) [$1\bar{1}0$] section of a roughened (110) surface. (b) The surface relief is characterized by the matrix of heights of top sites (integer numbers). Free top atoms marked by an asterisk are allowed to move. Reprinted from Ref. [30].

B. CO adsorption

We describe the adsorbate on the surface by mean field equations. This approach can be justified by the fact that CO molecules diffuse very rapidly on the Pt(110) surface. It is estimated that at low pressures there are about 10^6 site changes of an adsorbed CO molecule per adsorption event [33]. The quantitative measure of CO adsorption is the CO coverage, which can be also interpreted as the probability to find a CO molecule at some surface site. The averaged macroscale CO coverage θ_{CO} is governed by the following equation:

$$\frac{d\theta_{\text{CO}}}{dt}=k_a p_{\text{CO}}(1-\theta_{\text{CO}})-k_d\theta_{\text{CO}}, \tag{1}$$

where k_a and k_d are adsorption and desorption rate constants, respectively, and p_{CO} is the CO partial pressure in the gas phase. Thus, the occupancy of surface sites by CO molecules can be defined by the thermodynamical probability estimated from macroscopic equilibrium data. The CO desorption constant k_d depends exponentially on the CO chemisorption energy $E^{\text{Pt-CO}}$:

$$k_d=\nu_d\exp(-E^{\text{Pt-CO}}/k_BT). \tag{2}$$

The Pt atoms on the (110) surface are characterized by different coordination numbers varying from 5 to 11, and the values of $E^{\text{Pt-CO}}(n)$ at different Pt atoms may be distinct. Thus, Eq. (1) can be rewritten in the following form:

$$\frac{d\theta_{\mathrm{CO}}(n)}{dt} = k_a p_{\mathrm{CO}}[1 - y_{\mathrm{CO}}(n)] - k_d(n)\theta_{\mathrm{CO}}, \qquad (3)$$

where $\theta_{\mathrm{CO}}(n)$ is the total surface coverage of CO adsorbed on Pt atoms with the coordination number n, $y_{\mathrm{CO}}(n)$ is the local fraction of CO on n-coordinated Pt atoms and the desorption constant k_d is a function of $E^{\mathrm{Pt\text{-}CO}}(n)$ as in Eq. (2). It should be noted that a more precise equation would include CO exchange between different n-coordinated sites. However, this is irrelevant, if equilibrium CO distribution is achieved rapidly due to high diffusivity of CO molecules on the surface. We also assume that CO can desorb immediately when adsorption sites disappear due to reordering of the surface. The CO adsorption rate in Eq. (3) depends on the local fraction of CO on n-coordinated Pt atoms, defined as

$$y_{\mathrm{CO}}(n) = \theta_{\mathrm{CO}}(n)/x(n), \qquad (4)$$

where $x(n)$ is the total surface fraction of n-coordinated Pt atoms. To evaluate $x(n)$, we consider two atomic layers of Pt(110) shifted by half a lattice spacing in the [001] and $[1\bar{1}0]$ directions. Such a system consists of $2N^2$ atoms. At full CO saturation, the Pt(110) surface presents a close-packed 1×1 order. The ideal 1×1 surface consists of N^2 top atoms with $n=7$, where each top atom can only be bonded to one CO molecule. Then we define $x(n)=N_n/N^2$ with $x(7)=0.5$ for the 1×2 surface and $x(7)=1$ for the 1×1 structure.

The total CO coverage on the entire surface is defined as

$$\theta_{\mathrm{CO}}^{\mathrm{tot}} = \sum_{n=5}^{11} \theta_{\mathrm{CO}}(n). \qquad (5)$$

C. Transition probabilities for atomic jumps

We assume the energy of a Pt surface atom to be dependent on the Pt occupancy of the four adjacent sites in the same layer and to be modified by CO adsorption. Modification of the surface energy by CO is shown schematically in Fig. 3. On completely CO covered 1×2 patches of the surface, the modified energy of a Pt atom can be expressed in the form (in accordance with Fig. 3)

$$E = E_0 + E^{\mathrm{Pt\text{-}CO}}(n) + 4E_{NN}^{\mathrm{Pt\text{-}CO}} + E^{\mathrm{CO\text{-}CO}}, \qquad (6)$$

where the energy of a Pt atom of a clean surface is determined as $E_0 = n_v E_v + n_h E_h$ with n_v, n_h denoting the numbers of Pt-occupied vertical $[1\bar{1}0]$ and horizontal [001] positions in the same layer and E_v, E_h denoting the Pt-Pt binding energies between the adjacent atoms; $E_{NN}^{\mathrm{Pt\text{-}CO}}$ is the repulsive interaction energy between the central Pt atom (0) and CO molecules adsorbed on the NN positions in the layer below (1–4); $E^{\mathrm{CO\text{-}CO}}$ is the repulsive interaction energy between CO molecules attached to the Pt atom (0) and its adjacent sites (5,6). It should be noted, however, that the CO covered 1×2 state according to Eq. (6) and Fig. 3(c) is unstable due to strong repulsive interactions between the central Pt atom (0) and CO molecules attached to the (1–4) sites ($E_{NN}^{\mathrm{Pt\text{-}CO}} > 0$).

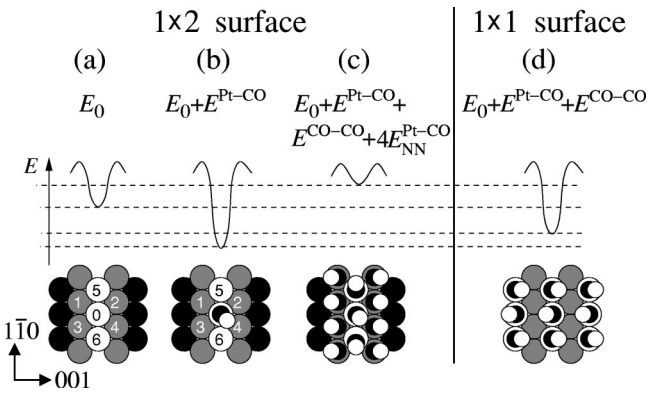

FIG. 3. Modification of the surface energy due to CO adsorption. The panels show relative energy levels for a clean 1×2 surface and different CO covered 1×2 and 1×1 states. Small double black-white circles denote CO molecules. (a) The central Pt atom (0) on a clean 1×2 surface has the energy E_0. (b) A CO molecule attached atop this atom decreases its energy by adding $E^{\mathrm{Pt\text{-}CO}}<0$. (c) Further adsorption of CO on the lower atomic layer (sites 1–4) destabilizes the central atom ($4E_{NN}^{\mathrm{Pt\text{-}CO}}>0$ is added). CO molecules adsorbed on the NN sites (5 and 6) interact with CO attached atop the central atom ($E^{\mathrm{CO\text{-}CO}}>0$ is added). (d) A CO-saturated 1×1 surface is more stable than the states shown in panels (a) and (c), since there is no CO adsorption on the (1–4) sites.

The adsorbate modification of activation barriers for Pt atom jumps can be taken into account in a similar way: CO molecules adsorb on the sites which are adjacent to the path of migrating Pt atom and increase the energy of transition state, as shown schematically in Fig. 4(a). Since the CO molecule van der Waals diameter (3.2 Å) is larger than the Pt lattice constant (2.78 Å in the [110] direction), diffusing Pt atoms cannot avoid interactions with CO molecules. As illustrated in Fig. 4(b), the displacements along or across $[1\bar{1}0]$ direction may be inhibited by two CO molecules adsorbed on the two NN sites on the layer below (marked by I and II in the figure). The LF hopping can be inhibited by the CO adsorption on the three adjacent sites (I,II,III) as shown in Fig. 4(c), whereas the atom hopping in the diagonal way may interact with only one CO molecule [see Fig. 4(d)]. Thus, we define the increase of activation barrier E_i^a of the vertical, horizontal, diagonal, and LF jumps on the CO covered surface, according to Figs. 4(b)–4(d), as

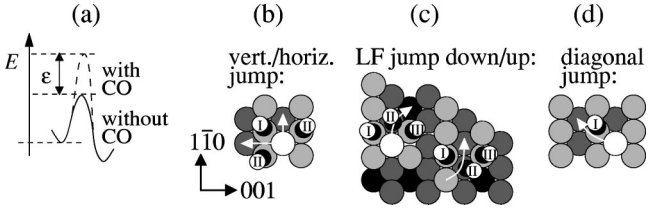

FIG. 4. Modification of the activation barriers due to CO adsorption. (a) Schematic increase of the transition state energy. (b) The vertically/horizontally hopping Pt atom may interact with two CO molecules marked by I, II. (c) The LF hopping can be inhibited by three CO molecules attached to adjacent sites marked by I, II, III. (d) The diagonal jump can be inhibited by one CO molecule (marked by I).

$$E_i^a = \begin{cases} E^0_{\text{vert/hor}} + 2\varepsilon^{\text{Pt-CO}} \\ E^0_{\text{diag}} + \varepsilon^{\text{Pt-CO}} \\ E^0_{\text{LF}} + 3\varepsilon^{\text{Pt-CO}}, \end{cases} \tag{7}$$

where $E^0_{\text{vert/horiz}}$, E^0_{diag}, E^0_{LF} are the transition state energies of Pt atom on a clean Pt(110) surface and $\varepsilon^{\text{Pt-CO}}$ is the correction modeling repulsive interaction between the Pt atom and CO molecules adsorbed on the adjacent sites.

The rate of single atomic step (hopping) on the clean surface is expressed in the Arrhenius form:

$$r_i = \nu_h \exp(-\Delta E_i / k_B T), \tag{8}$$

where $\Delta E_i = E_i^a - E_0$ is the activation barrier of ith hopping with i="vert," "hor," "diag," "LF up," or "LF down." Each hopping event on the surface occurs on the average once in a time interval $t_i = 1/r_i$. The characteristic time of the fastest step $\Delta t = 1/r_{\max} = 1/r(\Delta E_{\min})$ can be identified with the Monte Carlo step (MCS), i.e., the number of attempts equal to the surface lattice dimension $(2N^2)$. This allows us to translate MC units to real time, and probabilities of MC jumps to actual reaction rates. The probability of an atomic step P_i is defined as

$$P_i = r_i / r_{\max} = t_{\min}/t_i = \exp[-(\Delta E_i - \Delta E_{\min})/k_B T]. \tag{9}$$

This means that each free atom on the surface lattice moves on the average once via the ith path with the probability P_i during the physical time interval Δt.

We define a correction to the transition probability arising due to interactions with CO molecules as a multiplying factor, which is equal to 1 for the adsorbate-free configuration ($\theta_{\text{CO}} = 0$) and $\exp(\mathcal{H}/k_B T)$ for the CO covered state ($\theta_{\text{CO}} = 1$) with $\mathcal{H}$ modeling the modification of the energy or activation barrier ($\mathcal{H}$ may be positive or negative depending on the interaction type). According to the scheme shown in Fig. 3, the corrections to the atomic surface energy arising due to CO adsorption on the (0–6) sites are taken into account in the following way:

$$p_1 = (1-\theta_0) + \theta_0 \exp[E^{\text{Pt-CO}}(n)/k_B T], \tag{10}$$

$$\begin{aligned} p_2 = {} & \prod_{i=1}^{4} \theta_i \exp(4E^{\text{Pt-CO}}_{NN}/k_B T) \\ & + \sum_{i=1}^{4} \left((1-\theta_i) \prod_{j=1, j\neq i}^{4} \theta_j \right) \exp(3E^{\text{Pt-CO}}_{NN}/k_B T) \\ & + \sum_{i=1}^{4} \sum_{j=i+1}^{4} \left((1-\theta_i)(1-\theta_j) \prod_{k=1, k\neq i, k\neq j}^{4} \theta_k \right) \\ & \times \exp(2E^{\text{Pt-CO}}_{NN}/k_B T) + \sum_{i=1}^{4} \left(\theta_i \prod_{j=1, j\neq i}^{4} (1-\theta_j) \right) \\ & \times \exp(E^{\text{Pt-CO}}_{NN}/k_B T) + \prod_{i=1}^{4} (1-\theta_i), \end{aligned} \tag{11}$$

$$p_3 = (1 - \theta_0\theta_5\theta_6) + \theta_0\theta_5\theta_6 \exp(E^{\text{CO-CO}}/k_B T), \tag{12}$$

$$p = p_1 p_2 p_3, \tag{13}$$

where $\theta_l = y_{\text{CO}}(n)$, the index l runs from 0 to 6 and labels the NN atoms with the coordination number n. These expressions have been obtained for intermediate coverages $[0 \leqslant \theta_{\text{CO}}(n) \leqslant 1]$.

Similarly, one can derive the corrections to activation barriers on a CO covered surface. The following modifications have been included.

(1) *Vertical or horizontal displacement:*

$$\begin{aligned} b = {} & \theta_{\text{I}}\theta_{\text{II}} \exp(2\varepsilon^{\text{Pt-CO}}/k_B T) + [\theta_{\text{I}}(1-\theta_{\text{II}}) \\ & + (1-\theta_{\text{I}})\theta_{\text{II}}] \exp(\varepsilon^{\text{Pt-CO}}/k_B T) + (1-\theta_{\text{I}})(1-\theta_{\text{II}}). \end{aligned} \tag{14}$$

(2) *Diagonal displacement*:

$$b = (1-\theta_{\text{I}}) + \theta_{\text{I}} \exp(\varepsilon^{\text{Pt-CO}}/k_B T). \tag{15}$$

(3) *Vertical jump up/down to the layer above/below (LF)*:

$$\begin{aligned} b = {} & \prod_{i=\text{I}}^{\text{III}} \theta_i \exp(3\varepsilon^{\text{Pt-CO}}/k_B T) + \sum_{i=\text{I}}^{\text{III}} \left((1-\theta_i) \prod_{j=\text{I}, j\neq i}^{\text{III}} \theta_j \right) \\ & \times \exp(2\varepsilon^{\text{Pt-CO}}/k_B T) + \sum_{i=\text{I}}^{\text{III}} \left(\theta_i \prod_{j=\text{I}, j\neq i}^{\text{III}} (1-\theta_j) \right) \\ & \times \exp(\varepsilon^{\text{Pt-CO}}/k_B T) + \prod_{i=\text{I}}^{\text{III}} (1-\theta_i). \end{aligned} \tag{16}$$

Here $\theta_l = y_{\text{CO}}(n)$ and the site numbering (l=I, II, or III) is proceeded according to Figs. 4(b)–4(d).

The final form of the transition probability reads

$$P_i = \exp\left(-\frac{\Delta E_i - \Delta E_{\min}}{k_B T} \right) p b^{-1}. \tag{17}$$

It should be noted that in limiting cases the transition probability has a conventional form: for $\theta^{\text{tot}}_{\text{CO}} = 0$ the value of P_i is defined by Eq. (9). In the case of full CO saturation (i.e., the unstable CO covered 1×2 state), P_i includes the activation barrier $\Delta E_i = E_i^a - E$ defined by Eqs. (6) and (7).

IV. SIMULATION AND DISCUSSION

A. Estimation of the model parameters

Estimation of the model parameters is based on the available literature data adjusted when necessary to fit macroscopic experimental results. First, we define the parameters governing the CO adsorption on Pt(110). DFT calculations and experimental studies of CO adsorption under low-pressure conditions [16,34] have revealed selectivity of CO molecules with respect to different Pt surface configurations. The dependence of the binding energy $E^{\text{Pt-CO}}(n)$ on the Pt coordination number n can be approximated by a simple linear form [16] shown in Table II and Fig. 5. The average value of $E^{\text{Pt-CO}}(n)$ agrees with macroscopic data for CO desorption: $E^{CO}_{des} = -1.4$ eV [33] and $E^{CO}_{des} = -1.651$ eV [5].

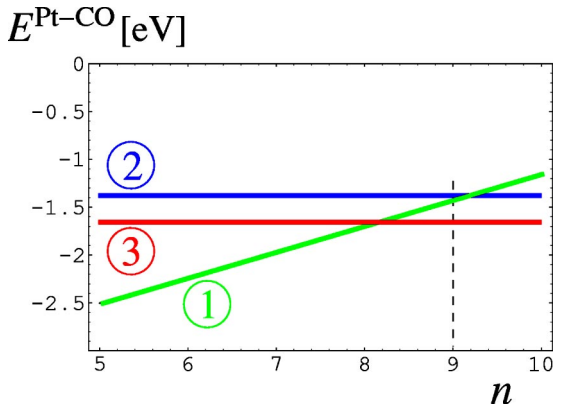

FIG. 5. Dependence of CO chemisorption energies on the coordination number of Pt atoms. The inclined line (1) is a linear fit to the data in Ref. [16]; the horizontal lines (2) and (3) show the average macroscopic values of $E^{\text{Pt-CO}}$ provided by Refs. [4,33], respectively.

The Pt-Pt and Pt-CO interaction energies used in our computations (E_v, E_h, and $E^{\text{Pt-CO}}$) are taken from Refs. [4,16,33], see Table II. The rest of the model parameters are presented in Tables III and IV. Since the values of activation barriers obtained by different methods can vary even for the same jumps (as shown in Table II), we have assumed the transition state energies for the vertical, horizontal, and LF jumps (E^0_{vert}, E^0_{hor}, and $E^0_{\text{LF up/down}}$, respectively) to be equal, whereas E^0_{diag} is assumed to be slightly higher. The barriers for the adatom diffusion obtained from STM [14,15], DFT calculations [22,23], and our fit are compared in Fig. 6, which shows the relative energy levels. In Refs. [14,15,22,23], the energy of the initial state of the hopping atom is defined in such a way that it corresponds to the zero level. The energy of this atom on a 1×1 patch of the surface is about 0.2–0.3 eV [14,15,23]. Since we take into account only the Pt-Pt interactions in one layer, a single atom on the 1×1 surface has the energy $E_0=0$ and the initial state of the hopping atom shown in Fig. 6 is characterized by the energy $E_0=E_v+2E_h=-0.125$ eV. Therefore, the activation barrier of the atom migrating on the 1×1 surface is much higher than that obtained by Kürpick ($E^a_{\text{vert}}=0.53$ eV [23]). At the same time, the discrepancy in the values of activation barriers proposed in Refs. [14,15,22,23] cannot be resolved by choosing appropriate Pt-Pt energy interactions. One can conclude that defining full atomic energy through a sum of Pt-Pt

TABLE III. Transition state energies E^0_i, minimum activation barrier ΔE_{min}, and preexponent factor of the hopping rates ν_h used in the simulation.

Parameter	Value	Reference
$E^0_{\text{vert}}=E^0_{\text{hor}}$	0.91 eV	[1,14,15,22,23],
$E^0_{\text{LF-up}}=E^0_{\text{LF-down}}$		Fit (see Fig. 6)
E^0_{diag}	0.92 eV	
ΔE_{min}	0.81 eV	[14]
ν_h	$10^{10.7}$ s^{-1}	[12–15]

TABLE IV. Two sets of the model parameters used in the simulations: CO chemisorption energy $E^{\text{Pt-CO}}$, corrections to the surface energy and activation barriers due to CO adsorption ($E^{\text{Pt-CO}}_{NN}$ and $\varepsilon^{\text{Pt-CO}}$, respectively) and macroscopic adsorption parameters k_a and ν_d.

Parameter	Case	Value	Reference
$E^{\text{Pt-CO}}$	(i)	Linear ($5\leqslant n\leqslant10$)	[16]
	(ii)	-1.4 eV ($5\leqslant n\leqslant9$)	[33]
$E^{\text{Pt-CO}}_{NN}$	(i)	0.19 eV	Fit
	(ii)	0.07 eV	Fit
$\varepsilon^{\text{Pt-CO}}$	(i)	0.15 eV	Fit
	(ii)	0.07 eV	Fit
k_a	(i),(ii)	0.47×10^5 mbar^{-1} s^{-1}	[4], fit
ν_d	(i)	8×10^{16} s^{-1}	[4], fit
	(ii)	5×10^{13} s^{-1}	[33]

binding energies between NN atoms in the same layer is not sufficiently precise.

Although the basic parameters of our model are taken from the available literature data, the model also includes several free parameters ($E^{\text{Pt-CO}}_{NN}$,$\varepsilon^{\text{Pt-CO}}$), which have been fitted from the dynamical considerations. Excessive increase of the correction $E^{\text{Pt-CO}}_{NN}$ destabilizes top Pt atoms and leads to chaotic migration of adatoms on the surface reducing tendency to the 1×1 state formation at high $\theta^{\text{tot}}_{\text{CO}}$. Extremely high $\varepsilon^{\text{Pt-CO}}$ values block adatom migration even at low CO

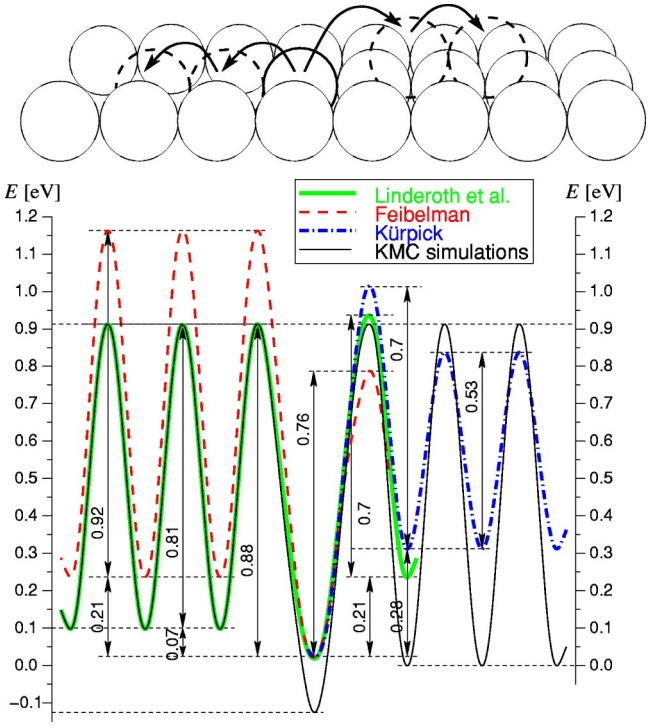

FIG. 6. (Color online) Comparison of the activation barriers for single adatom jumps according to Linderoth *et al.* [14,15] (thick solid line), Feibelman [22] (dashed line), and Kürpick [23] (dash-dot line). Our fit used in the KMC simulations is shown by the thin solid line.

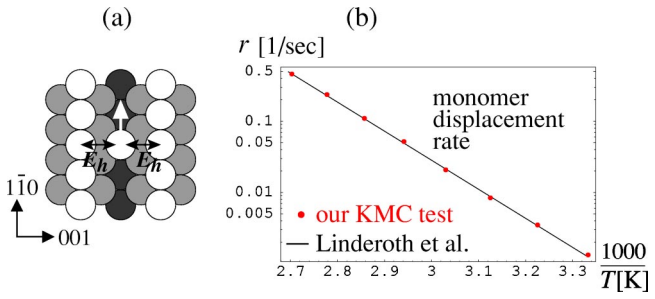

FIG. 7. (a) Scheme of a monomer migrating along the [$\bar{1}$10] direction in a 1×2 channel. This atom is characterized by the highest energy due to repulsive interactions with horizontal (wall) atoms ($E_h>0$). (b) The monomer displacement rate vs inverse temperature $1/T$. The simulation results are shown by points. The solid line shows the fit to STM observations: $r_{\mathrm{mon}}=10^{10.7}\exp(-0.81/k_BT)$ [14]. Computation lattice: 2×50^2 atoms.

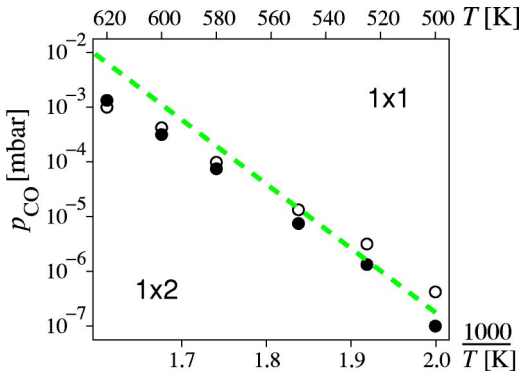

FIG. 8. The boundary between preferred 1×2 and 1×1 structures in the (p_{CO},T) plane. The dashed line denotes the fit to macroscopic experimental data on 1×2→1×1 transition [35]. The results of our KMC simulations with $E^{\mathrm{Pt\text{-}CO}}=-1.4$ eV are shown by the open dots and those with linear $E^{\mathrm{Pt\text{-}CO}}(n)$ by the filled dots. Computation lattice: 2×50^2 atoms.

coverages on the surface. Therefore, the values of these corrections have been chosen in such a way that the SPT is initiated at realistic CO exposure doses and relaxation to the close-packed 1×1 state occurs under high CO coverages.

Table IV shows two sets of the parameters adjusted when the CO chemisorption energy depends linearly on Pt coordination number [case (i)] and $E^{\mathrm{Pt\text{-}CO}}$ is constant [case (ii)]. Both forms of the CO chemisorption energy require fitting some free parameters ($E_{NN}^{\mathrm{Pt\text{-}CO}}$ and $\varepsilon^{\mathrm{Pt\text{-}CO}}$). The linear form of $E^{\mathrm{Pt\text{-}CO}}(n)$ is more realistic, but the use of a constant value of $E^{\mathrm{Pt\text{-}CO}}$ allows us to simplify the model by reducing the number of equations for CO coverage. These two cases will be compared in the following section.

The efficiency of the proposed algorithm, as well as validity of translation to real time units, depends on the definition of the normalizing value ΔE_{min}. The most natural choice for ΔE_{min} might be just the minimum activation barrier calculated for all possible configurations and hopping events. We assume that on a clean Pt(110) surface, ΔE_{min} is equal to $E_{\mathrm{vert}}^0-E_{\mathrm{mon}}=0.81$ eV [14], i.e., the activation barrier for a monomer displacement in 1×2 channels. Such a monomer shown schematically in Fig. 7(a) presents the most unstable configuration on a defect 1×2 surface and this was shown by STM experiments [14].

B. Computation results

Computations have been carried out according to the algorithm presented in Appendix. We start with a simulation of dynamics of single adatoms on a clean nonperfect 1×2 surface without the adsorbate. Our numerical tests with the minimum activation barrier $\Delta E_{\mathrm{min}}=0.81$ eV show very good agreement of the calculated monomer displacement rate r_{mon} with the experimental one, as shown in Fig. 7(b). This result can serve as an evidence for the validity of the proposed algorithm.

One can take note, however, of a large difference between activation barriers for allowed steps on a clean and CO covered surface. This difference can arise due to the corrections $E_{NN}^{\mathrm{Pt\text{-}CO}}$ and $\varepsilon^{\mathrm{Pt\text{-}CO}}$ for hoppings on CO covered spots of the surface. In this case, the corresponding transition rates may differ by several orders of magnitude. The activation barriers of some CO-induced hoppings may be essentially lower than ΔE_{min}. Nevertheless, our simulations with the normalizing value ΔE_{min} chosen for a clean surface (0.81 eV) reproduces the initiation of the 1×2→1×1 reconstruction under $p_{\mathrm{CO}}>0$ on a correct time scale. This normalization choice means that all atomic steps with the activation barrier $\Delta E_i<\Delta E_{\mathrm{min}}$ occur with the same probability $P_i=1$. The rates of the CO-induced fastest steps are actually underestimated when the KMC algorithm defined in this way is implemented, but this should not affect the kinetic of reconstruction in an essential way, since the phase transition occurs on a correct time scale. However, in low temperature simulations, the value of ΔE_{min} should be decreased in order to provide an appropriate time step in integration of Eq. (3).

Simulations of the CO-lifted reconstruction on a perfect 1×2 surface have been carried out under the following alternative assumptions: (i) CO chemisorption energy depends on the coordination of Pt atoms according to Ref. [16]; (ii) $E^{\mathrm{Pt\text{-}CO}}$ is the average value estimated from the macroscopic data. In the simulations including the linear form of $E^{\mathrm{Pt\text{-}CO}}(n)$, we use a preexponential factor of the CO desorption rate close to that of Ref. [4], $\nu_d=8\times10^{16}$ s^{-1}, since the average value of $E^{\mathrm{Pt\text{-}CO}}(n)$ fits the macroscale CO desorption energy value (−1.651 eV) provided in this work.

The simulation results for SPT in extended temperature range are compared with the experimental data [35] in Fig. 8, which shows the boundary between preferred 1×2 and 1×1 structures in the p_{CO}-T plane. The experimental boundary denotes the conditions corresponding to the completion of the 1×2→1×1 SPT. The simulations of relaxation process were carried out for different temperatures until the stationary state was reached for each p_{CO} value. The dots in Fig. 8 mark the critic values of p_{CO} and T at which the stationary surface state does not contain 1×2 spots. The simulations started with random initial conditions (atoms of the upper layer were distributed randomly and atomic quantity ratio for the first two upper layers was ≈1/2). The two forms of $E^{\mathrm{Pt\text{-}CO}}$ have been checked. Calculations with the linear de-

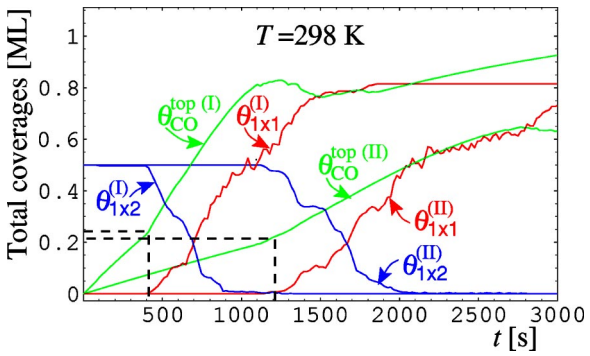

FIG. 9. (Color online) Simulated dynamics of CO adsorption and reconstruction vs CO dosage at $T=298$ K and $p_{CO}=5\times10^{-9}$ torr (I), $p_{CO}=1.5\times10^{-9}$ torr (II). Both the linear dependence $E^{Pt\text{-}CO}(n)$ and constant $E^{Pt\text{-}CO}$ provide similar results. The simulations started with a perfect 1×2 surface. The total surface fractions of CO, 1×1 and 1×2 phases are shown. At both pressures, reconstruction is initiated at the CO exposure dose $\sim 2L$ and when θ_{CO}^{tot} reaches $\sim$0.2–0.25. Computation lattice: 2×50^2 atoms.

pendence of $E_{NN}^{Pt\text{-}CO}(n)$ and the respective data from Table IV [case (i)] show that 1×1 patches completely cover the surface at the conditions similar to the experimental ones. Some discrepancy, however, arises at higher T. The simulations, assuming $E^{Pt\text{-}CO}=-1.4$ eV for Pt atoms with $5\leqslant n\leqslant 9$ and the respective macroscale data ($\nu_d=5\times10^{13}\,s^{-1}$) provided by Ref. [33], also demonstrate a good agreement with the experiments in the reconstruction diagram at T varied from 500 K to 620 K, as shown in Fig. 8. The values of the activation energy corrections $E_{NN}^{Pt\text{-}CO}$ and $\varepsilon^{Pt\text{-}CO}$ used in this case are presented in Table IV [case (ii)]. Using a constant value of $E^{Pt\text{-}CO}$ can be justified by assuming that in the high temperature range, random migration of CO molecules on the surface will eliminate the energy gain associated with localization of CO molecules at the sites with lower coordination numbers. The experimentally detected displacement of single step atoms forming holes may suggest that CO molecules can also attach to the high-coordinated sites in the layer below ($n=8,9$) even at low CO coverage. This assumption can significantly simplify the model by introducing a constant average value of the CO chemisorption energy instead of a linear $E^{Pt\text{-}CO}(n)$.

The simulations for room temperature conditions reproduce very well the $1\times2\rightarrow1\times1$ reconstruction dynamics observed in the STM experiments [34]. At $p_{CO}=1.5\times10^{-9}$ torr and $p_{CO}=5\times10^{-9}$ torr, the reconstruction begins at realistic values of the CO exposure dose (about $p_{CO}\times t\times10^6$ torr s $\approx 2L$), as shown in Fig. 9. Both the linear and constant $E^{Pt\text{-}CO}$ provide the similar dynamical behavior. In calculations for $T=298$ K, the normalization value ΔE_{min} is chosen as $\Delta E_{min}<0.81$ eV, since the time interval corresponding to 1 MCS is too large [$\Delta t=1/r_{max}(0.81)=998.3$ s] at $T=298$ K and cannot be used in integration of the mean field part of the model. Therefore, we reduce ΔE_{min} to 0.6 eV in order to provide a normal time step ($\Delta t=0.28$ s). Further decrease does not affect significantly the simulation results, but steeply increases the computation time.

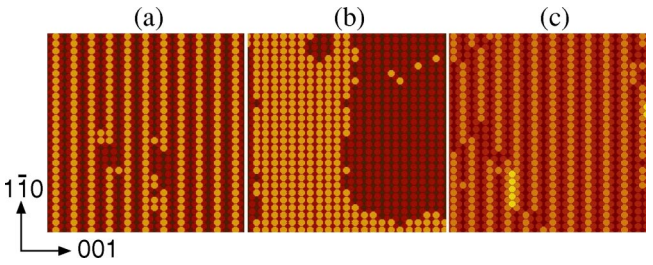

FIG. 10. (Color online) Simulation of reversible $1\times2\rightarrow1\times1\rightarrow1\times2$ reconstruction. (a) Onset of reconstruction. (b) Patches of the 1×1 surface. (c) The 1×2 surface with defects obtained from the state (b) after switching to $p_{CO}=0$. Both the linear dependence $E^{Pt\text{-}CO}(n)$ and constant $E^{Pt\text{-}CO}$ provide the same reconstruction scenario. Computation lattice: 2×50^2 atoms.

In both the studied cases, the $1\times2\rightarrow1\times1$ reconstruction is initiated via defect formation followed by hole eating process, as shown in Fig. 10(a), leading eventually to a terraced 1×1 structure [Fig. 10(b)]. The reconstruction mechanism shown in Fig. 10 is similar at all p_{CO} and T values along both simulated phase transition boundaries presented in Fig. 8. After the CO pressure has been lowered stepwise to zero, reverse $1\times1\rightarrow1\times2$ reconstruction restores the 1×2 structure, which is now not regular, but contains a number of defects, as shown in Fig. 10(c).

The linear dependence of $E^{Pt\text{-}CO}(n)$ from Ref. [18] has been derived on the base of PW91-gradient approximation method [36,37] which is known to give overestimation in CO chemisorption energies [38]. In this regard, our study with the constant $E^{Pt\text{-}CO}$ taken from Ref. [33] can be relevant.

A recent STM study of CO adsorption on the Pt(110) surface [34] has detected anisotropic nanoscale clusters of the 1×1 surface phase under different p_{CO} varied in an extremely wide range (10^{-9}–10^3 mbar). At low CO pressures (10^{-9}–10^{-5} mbar) the displaced Pt atoms form a channel-like structure extended in the [001] direction. An increase of p_{CO} to $\sim10^{-2}$–1 mbar smoothes edges of the 1×1 clusters. Higher CO pressures ($\sim10^3$ mbar) result in a zigzag structure of Pt atomic order characterized by sharp edges of the clusters extended in the $[1\bar{1}0]$ direction. Such a difference in anisotropy of the 1×1 islands under varied p_{CO} can be attributed to distinct CO chemisorption energies on different configurations of island boundaries. At low CO pressures, CO adsorption on low-coordinated Pt atoms is favorable, but an increase of p_{CO} causes CO molecules to adsorb also on high-coordinated Pt atoms leading to the formation of kinks on boundaries of islands. One can also suggest that $E^{Pt\text{-}CO}$ on 9-coordinated atoms of (111) facets differs from $E^{Pt\text{-}CO}(9)$ on the (100) surface section and, thus, the anisotropy can be achieved.

V. CONCLUSIONS

We present a kinetic MC model which takes into account realistic Pt-Pt interactions between the surface atoms and activation barriers for hopping of single Pt atoms both for a clean and CO covered surface. Since the diffusion rate of CO

molecules on the surface is much higher than displacement rates of single Pt adatoms, the CO adsorption on Pt(110) is described in a mean field approximation. A nonuniform CO distribution on different surface configurations is taken into account. For this purpose, we combine a system of equations of a Langmuir-Hinshelwood type describing the total surface fraction of CO adsorbed on Pt sites with specific coordination numbers. Distinct CO coverages are achieved due to different CO desorption energies on Pt atoms with different coordination numbers. The simulated reversible reconstruction process induced by CO adsorption occurs on a realistic time scale at the experimental conditions. The computation lattice represents a 3D relief of Pt(110) surface. In the case of CO adsorption, the SPT mostly involves an atomic transport between several atomic layers (up to four). The simulated CO-lifted reconstruction from a clean 1×2 surface to a 1×1 state, as well as the reverse SPT without CO, does not cause significant increase of roughening on the surface. One can expect, however, that an inclusion of oxygen adsorption in the CO/Pt(110) system will cause kinetic instabilities which will result in development of roughening and faceting [9,10,39] characterized by much larger height dispersion of top Pt atoms. In this case, it would be more convenient to combine the KMC algorithm with only one equation for the CO coverage including the average value of CO chemisorption energy. Applicability of this approach has also been proved in the present work. The model for faceting in the CO oxidation reaction will be presented in a forthcoming paper.

ACKNOWLEDGMENTS

This research was supported by the German-Israeli Science Foundation.

APPENDIX

Computation algorithm

In this Appendix, the computation loop for one MCS is presented. The KMC algorithm shifts the atoms between lattice nodes according to the following rules.

(1) A random free (not covered by any atom in the higher layer) atom is selected on the lattice.

(2) For the chosen free atom, possible jump positions are determined. Any atom can jump only to a free adjacent position in the same layer, in the layer above or below, as shown in Fig. 1. Each of 16 possible positions shown in Fig. 1 has to be checked. An accepted atomic position should be propped up by four corner atoms of the lower layer. Periodic boundary conditions are applied at the lattice boundaries.

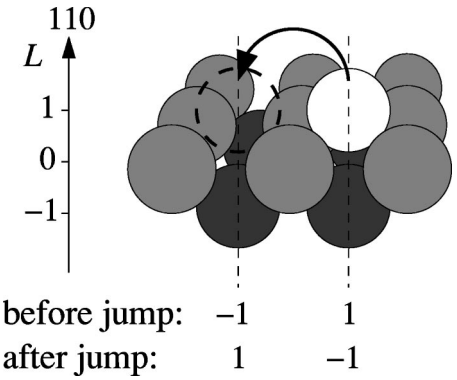

FIG. 11. Change of the atomic layer tag L at two lattice nodes associated with one jump.

(3) The coordination numbers of the chosen atom, NN atoms, and sites adjacent to each ith path are determined. The energy of the current position, E, and the activation barriers for each possible jump, ΔE_i^a, are evaluated by Eqs. (6) and (7), where CO coverages on sites with different n are taken from the previous time step. The set of transition probabilities P for all possible jumps is computed according to Eq. (17).

(4) A random number R uniformly distributed between zero and unity is drawn, and a new position is chosen randomly among the available vacant sites with $P_i > R$. If $P_i < R$ for each ith path, no jump is executed and the calculation returns to step 1.

(5) After a new position is selected, the atom is removed from the old position, i.e., the layer tag of the respective site is reduced by two; the layer tag of the new site is increased by two (see Fig. 11), and the computation returns to step 1.

This procedure is repeated $2N^2$ times. Following this, time is incremented by Δt specified for the MF part of the model. The numerical data are collected: $x(n)$, fractions of the surface phases $\theta_{1\times1}$ and $\theta_{1\times2}$. CO coverages $\theta_{\mathrm{CO}}(n)$ with $n=5-10$ for the next time step are calculated according to Eq. (3) with updated $x(n)$.

[1] T. Gritsch, D. Coulman, R.J. Behm, and G. Ertl, Phys. Rev. Lett. **63**, 1086 (1989).

[2] S. Schwegmann, W. Tappe, and U. Korte, Surf. Sci. **334**, 55 (1995).

[3] R.K. Sharma, W.A. Brown, and D.A. King, Surf. Sci. **414**, 68 (1998).

[4] K. Krischer, M. Eiswirth, and G. Ertl, J. Chem. Phys. **96**, 9161 (1992).

[5] I.K. Robinson, P.J. Eng, C. Romainczyk, and K. Kern, Surf. Sci. **367**, 105 (1996).

[6] P. Fery, W. Moritz, and D. Wolf, Phys. Rev. B **38**, 7275 (1988).

[7] M.A. Krzyzowski, P. Zeppenfeld, C. Romainczyk, R. David, G. Comsa, K.E. Kuhnke, and K. Kern, Phys. Rev. B **50**, 18 505 (1994).

[8] R. Imbihl and G. Ertl, Chem. Rev. (Washington, D.C.) **95**, 697 (1995).

[9] S. Ladas, R. Imbihl, and G. Ertl, Surf. Sci. **197**, 153 (1988).

[10] S. Ladas, R. Imbihl, and G. Ertl, Surf. Sci. **198**, 42 (1988).

[11] M. Nowicki, A. Emundts, G. Pirug, and H.P. Bonzel, Surf. Sci. **478**, 180 (2001).

[12] T.R. Linderoth, S. Horch, E. Lægsgaard, I. Stensgaard, and F. Besenbacher, Surf. Sci. **402**, 308 (1997).

[13] T.R. Linderoth, S. Horch, E. Lægsgaard, I. Stensgaard, and F. Besenbacher, Phys. Rev. Lett. **78**, 4978 (1997).

[14] T.R. Linderoth, S. Horch, L. Petersen, S. Helveg, E. Lægsgaard, I. Stensgaard, and F. Besenbacher, Phys. Rev. Lett. **82**, 1494 (1999).
[15] T.R. Linderoth, S. Horch, L. Petersen, S. Helveg, M. Schønning, E. Lægsgaard, I. Stensgaard, and F. Besenbacher, Phys. Rev. B **61**, R2448 (1999).
[16] P. Thostrup, E. Christoffersen, H.T. Lorensen, K.W. Jacobsen, F. Besenbacher, and J.K. Nørskov, Phys. Rev. Lett. **87**, 126102 (2001).
[17] P. Hanesch and E. Bertel, Phys. Rev. Lett. **79**, 1523 (1997).
[18] GuoCe Zhuang and Wei Wang, Phys. Lett. A **268**, 413 (2000).
[19] F. Montalenti and R. Ferrando, Phys. Rev. Lett. **82**, 1498 (1999).
[20] T. Yamaghishi, K. Takahashi, and T. Onzawa, Surf. Sci. **445**, 18 (2000).
[21] K. Swamy, E. Bertel, and I. Vilfan, Surf. Sci. Lett. **425**, L369 (1999).
[22] P.J. Feibelman, Phys. Rev. B **61**, R2452 (2000).
[23] U. Kürpick, Phys. Rev. B **63**, 045409 (2001).
[24] R. Imbihl, A.E. Reynolds, and D. Kaletta, Phys. Rev. Lett. **67**, 275 (1991).
[25] R.J. Gelten, A.P.J. Jansen, R.A. van Santen, J.J. Lukkien, J.P.L. Segers, and P.A.J. Hilbers, J. Chem. Phys. **108**, 5921 (1998).
[26] V.P. Zhdanov and B. Kasemo, J. Chem. Phys. **114**, 5351 (2001).
[27] V.P. Zhdanov, Surf. Sci. Rep. **287**, 1 (2002).
[28] E. Christoffersen, P. Stoltze, and J.K. Nørskov, Surf. Sci. **505**, 200 (2002).
[29] M. Monine and L.M. Pismen, Catal. Today **70**, 311 (2001).
[30] M. Monine and L.M. Pismen, Phys. Rev. E **66**, 051601 (2002).
[31] D.P. Landau and K. Binder, *A Guide to Monte-Carlo Simulation in Statistical Physics* (Cambridge University Press, Cambridge, 2000).
[32] Keh-Dong Shiang and Tien T. Tsong, Phys. Rev. B **51**, 5522 (1995).
[33] C. Reichert, J. Starke, and M. Eiswirth, J. Chem. Phys. **115**, 4829 (2001).
[34] P. Thostrup, E.K. Vestergaard, E. Lægsgaard, and F. Besenbacher, J. Chem. Phys. **118**, 3724 (2003).
[35] M. Eiswirth, P. Möller, K. Wetzl, R. Imbihl, and G. Ertl, J. Chem. Phys. **90**, 510 (1989).
[36] J.P. Perdew, J.A. Chevary, S.H. Vosko, K.A. Jackson, M.R. Pederson, D.J. Singh, and C. Fiolhais, Phys. Rev. B **46**, 6671 (1992).
[37] R.A. van Santen, *Theoretical Heterogeneous Catalysis* (World Scientific, Singapore, 1991).
[38] B. Hammer, L.B. Hansen, and J.K. Nørskov, Phys. Rev. B **59**, 7413 (1999).
[39] R. Imbihl, Mod. Phys. Lett. B **6**, 493 (1992).